Nanoscale

PAPER

Cite this: *Nanoscale*, 2014, **6**, 12690

Valley and spin dynamics in $MoSe_2$ two-dimensional crystals

Nardeep Kumar,[a] Jiaqi He,[b] Dawei He,[b] Yongsheng Wang*[b] and Hui Zhao*[a]

Received 27th June 2014,
Accepted 20th August 2014

DOI: 10.1039/c4nr03607g

www.rsc.org/nanoscale

We study valley and spin dynamics in monolayer molybdenum diselenide by polarization-resolved femtosecond transient absorption spectroscopy. Valley- and spin-polarized excitons are injected by a circularly polarized laser pulse, with an excess energy of 120 meV. Relaxation of the valley polarization is time-resolved by measuring dynamical circular dichroism of a linearly polarized probe pulse tuned to 790 nm, the peak of the exciton resonance of monolayer $MoSe_2$. We obtain a valley relaxation time of 9 ± 3 ps at room temperature, which is at least one order of magnitude shorter than the simultaneously measured exciton lifetime. The results illustrate potential applications of $MoSe_2$ in room-temperature valleytronic and spintronic devices.

1. Introduction

Semiconducting transition metal dichalcogenides, MX_2 (M=Mo, W; X=S, Se, Te), have drawn considerable attention since 2010.[1] Similar to graphene,[2] the weak van der Waals interlayer coupling in these layered crystals allows fabrication of atomically thin two-dimensional (2D) films.[3] These 2D crystals have properties that are remarkably different from their bulk counterparts,[4–6] and have shown potential applications in electronics[7–9] and optoelectronics.[10–14]

Due to their unique spin and valley properties,[15–17] MX_2 2D crystals have also emerged as promising materials for spintronics[18–20] and valleytronics,[21] where the spin degree of freedom or valley index of electrons is used for information processing. Fig. 1(a) shows a top view of the lattice structure of a MX_2 monolayer. It is composed of one layer of M atoms (blue circles) that is sandwiched by two layers of X (yellow circles). Since this lattice is not inversion symmetric, in momentum space the 6 energy valleys form two inequivalent sets, labeled as K and K′ in Fig. 1(b), respectively. Fig. 1(c) shows the conduction (C) and valence bands [V_A (spin 3/2), V_B (spin 1/2)] in K (left) and K′ (right) valleys, respectively. The large spin splitting in the valance bands (several hundreds of meV) is induced by the spin–orbital coupling in d orbitals of the X atoms.[22–24] The unique aspect of the spin properties in MX_2 2D crystals is that the spin and valley degrees of freedom of holes in the valance bands are inherently coupled: time-reversal symmetry and the lack of inversion symmetry in space dictate that the spin splitting at different valleys must be opposite.[15,25] As illustrated in Fig. 1(c), in the K valleys, the spin-down (spin −3/2) and spin-up (spin +1/2) holes occupy the V_A and V_B bands, respectively; while in the K′ valleys the spin occupation is the opposite. Since holes in opposite valleys carry opposite Berry curvatures and spin moments, a number

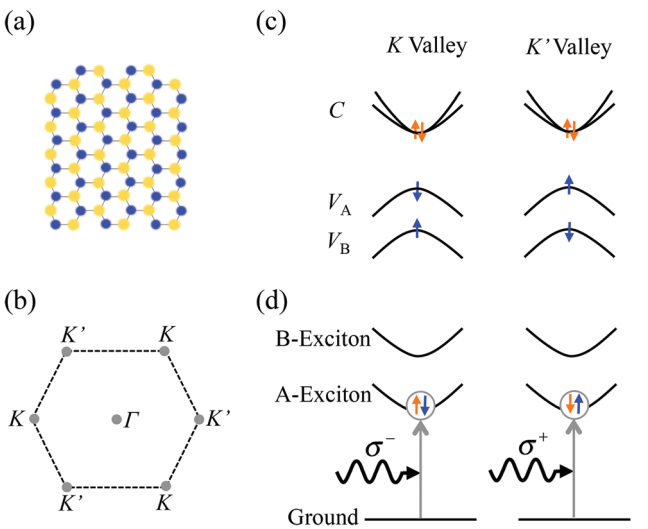

Fig. 1 (a) Lattice structure of MX_2 2D crystals. Each yellow circle represents two X atoms vertically separated. The blue circles indicate the plane of M atoms located between the two *X* planes. (b) Energy valleys K and K′ in momentum space. (c) Electronic structures in K (left) and K′ (right) valleys, showing the conduction (C) and valance (V_A and V_B) bands and their spin states (up and down arrows). (d) Spin configurations of the bright excitons in the two valleys and their coupling to circularly polarized light.

[a]*Department of Physics and Astronomy, The University of Kansas, Lawrence, Kansas 66045, USA. E-mail: huizhao@ku.edu; Fax: +1 785 864 5262; Tel: +1 785 864 1938*
[b]*Key Laboratory of Luminescence and Optical Information, Ministry of Education, Institute of Optoelectronic Technology, Beijing Jiaotong University, Beijing 100044, China*

of interesting phenomena resulted, such as spin and valley Hall effects.[15,17,26–29] In both valleys, the conduction bands (C) are degenerate near the bottom of the bands.

One important consequence of these spin and valley structures is the spin- and valley-selective optical coupling.[15–17] The optical properties of MX_2 2D crystals are dominated by excitons due to their large binding energies. Fig. 1(d) shows the two exciton bands, A and B, formed by the holes in V_A and V_B, respectively, with electrons in the conduction bands. Since in the K valleys only spin-down holes populate V_A, an A-exciton in the K valley is formed by a spin-down hole (−3/2) with either a spin-up (+1/2) or a spin-down (−1/2) electron. The former [shown in Fig. 1(d)] has a net spin of −1 (spin-down exciton) and therefore couples to σ^- photons, while the latter, with a net spin of −2, is a dark exciton that does not couple to photons (not shown). On the other hand, in the K′ valleys, a bright A-exciton is formed by a spin-up hole (+3/2) and a spin-down electron (−1/2), with a net spin of +1 (spin-up exciton), and hence couples to σ^+ photons. Based on these selection rules, a circularly polarized light can inject spin- and valley-polarized excitons in MX_2 2D crystals,[15–17] which then emit circularly polarized photoluminescence. This effect has been observed by several groups in steady-state photoluminescence experiments.[16,30–36] Dynamics of spin and valley polarized excitons have also been revealed in time-resolved photoluminescence[37] and transient absorption[38,39] measurements.

Here we demonstrate optical injection and detection of valley- and spin-polarized excitons in $MoSe_2$ monolayers at room temperature by polarization-resolved transient absorption measurements. We deduce a valley relaxation time of 9 ± 3 ps in monolayer samples at room temperature. Previous observations of valley polarization have mostly focused on one member of MX_2, MoS_2,[16,30–36,38,39] and were limited to low sample temperatures. Our results illustrate potential applications of $MoSe_2$ 2D crystals for room-temperature valleytronics and spintronics.

2. Experimental section

Thin flakes of $MoSe_2$ are mechanically exfoliated from bulk crystals, and then deposited on silicon substrates with a 90 nm SiO_2 layer. Monolayer flakes are first identified with an optical microscope, according to their optical contrasts,[40,41] and then confirmed by photoluminescence[42–44] and Raman spectroscopy.[42,44–47]

Fig. 2 illustrates the experimental setup. A left-circularly polarized (σ^+) pump pulse with a 730 nm central wavelength and 100 fs temporal width resonantly injects excitons into the sample. The pulse is tightly focused to about 1 μm and is located at the center of the monolayer flake to avoid any potential effects from the flake boundary. According to the selection rules illustrated in Fig. 1(d), spin-up excitons are injected into the K′ valleys. The dynamics of these excitons is probed by using a linearly polarized (x) pulse tuned to the A-exciton

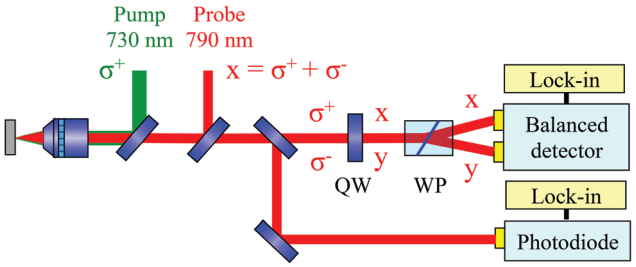

Fig. 2 Polarization-resolved differential reflection setup to measure pump-induced circular dichroism, which reflects spin and valley dynamics of excitons (QW: quarter-wave plate, WP: Wollaston prism).

resonance (790 nm), by utilizing the dynamic circular dichroism induced by the valley- and spin-polarized excitons.

It has been well established that an exciton population can change the absorption coefficient of a semiconductor by various mechanisms such as phase-space state filling, screening, bandgap renormalization, *etc.*[48] For low and even moderate densities, the change in absorption coefficient is proportional to the exciton density.[48] In our measurements, this change is monitored by differential reflection, which is defined as the relative change of the probe reflection induced by the excitons, $\Delta R/R_0 \equiv [R(N) - R_0]/R_0$, where $R(N)$ and R_0 are probe reflections with and without excitons, respectively.

The x-polarized probe has two circular components, σ^+ and σ^-, of equal magnitude. We first consider the σ^- component. The differential reflection of a σ^--polarized light can be written as

$$\frac{\Delta R^-}{R_0} = C_1 N_\downarrow + C_2 N_\uparrow, \quad (1)$$

where $N_\downarrow$ and $N_\uparrow$ are the densities of spin-down and spin-up excitons, respectively. The coefficients C_1 and C_2 describe the effectiveness of spin-down and spin-up excitons in altering the absorption of the σ^- probe. Here C_2 originates from spin-insensitive mechanisms, while C_1 is from both spin-insensitive and spin-sensitive processes. Hence, $C_1 > C_2$. That is, the spin-down excitons, or excitons in the K′ valley, are more efficient in altering the absorption of σ^- light. Similarly, the differential reflection of the σ^+ component,

$$\frac{\Delta R^+}{R_0} = C_1 N_\uparrow + C_2 N_\downarrow. \quad (2)$$

By measuring the sum and difference of these two components, we obtain

$$\frac{\Delta R^+}{R_0} + \frac{\Delta R^-}{R_0} = (C_1 + C_2)(N_\uparrow + N_\downarrow) = (C_1 + C_2)N, \quad (3)$$

and

$$\frac{\Delta R^+}{R_0} - \frac{\Delta R^-}{R_0} = (C_1 - C_2)(N_\uparrow - N_\downarrow) = (C_1 - C_2)S, \quad (4)$$

where N and S are the exciton and spin (valley) densities, respectively. Furthermore,

$$\frac{\Delta R^+ - \Delta R^-}{\Delta R^+ + \Delta R^-} = \frac{C_1 - C_2}{C_1 + C_2}\frac{S}{N} = \frac{C_1 - C_2}{C_1 + C_2}P, \quad (5)$$

where P is defined as spin and valley polarizations of the excitons.

As shown in Fig. 2, to separate the two circular components of the probe, a portion of the reflected probe is sent through a quarter-wave plate (QW) with the fast axis oriented such that it converts the two circular components to x and y linear polarizations. A Wollaston prism (WP) separates the two components, which are measured by the two photodiodes of a balanced detector. Since the balanced detector outputs a voltage that is proportional to the difference between the optical powers on the two detectors, it monitors the difference of the two differential reflections, and hence the spin density. This output is measured by a lock-in amplifier synchronized with a mechanical chopper in the pump arm, which modulates the pump intensity at about 3000 Hz. The other portion of the reflection probe is measured directly by another photodiode, which monitors the sum of the two spin systems, *i.e.* total exciton density.

3. Results and discussion

Fig. 3(a) shows the measured $\Delta R/R_0$ as a function of the probe delay after excitons are injected by a σ^+-polarized pump pulse with a central wavelength of 730 nm. The peak density of the injected excitons is about 5×10^{11} cm^{-2}, which is estimated from the pump fluence used and the absorption coefficient of the sample at the probe wavelength. Since $\Delta R/R_0$ measures the total exciton density, its decay reflects loss of exciton density due to recombination. After an initial rapid decay, which has a time constant of about 0.5 ps, the signal decreases slowly. A separate measurement over a longer time range (not shown) yields a relatively long decay time of 130 ps. We attribute the short time constant to thermalization and energy relaxation of excitons, and the long time constant to the exciton lifetime. Furthermore, when the laser spots are moved to a region of the substrate that is not covered by $MoSe_2$, no signal is detected under the same conditions. This verifies that the Si substrate makes a negligible contribution to the observed $\Delta R/R_0$.

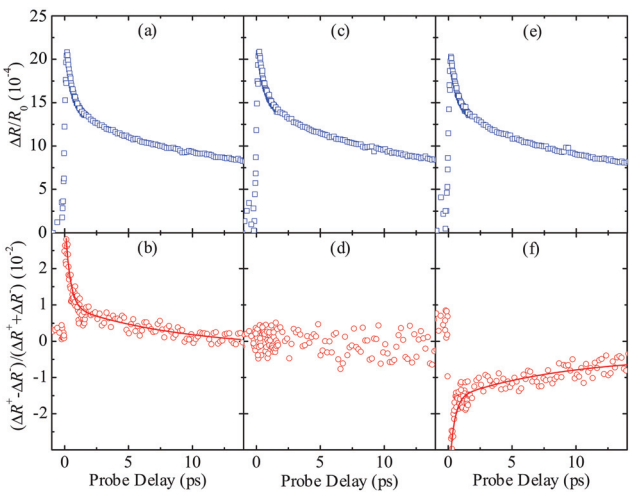

Fig. 3 Differential reflection (a, c, e) and the ratio between difference and sum of the two circular components (b, d, f) of monolayer $MoSe_2$ measured with pump pulses of σ^+ (a, b), x (c, d), and σ^- (e, f) polarizations, respectively.

Fig. 3(b) shows $(\Delta R^+ - \Delta R^-)/(\Delta R^+ + \Delta R^-)$ as a function of the probe delay. This quantity is obtained by measuring $\Delta R^+ - \Delta R^-$ and $\Delta R^+ + \Delta R^-$ simultaneously with the two detectors shown in Fig. 2, and then taking the ratio numerically. As shown in eqn (5), this quantity is proportional to the valley and spin polarizations of the excitons. Clearly, a positive polarization is injected by the pump, which decays quickly. We find that the decay can be described by a bi-exponential function (red line), with a short time constant of 0.36 ± 0.05 and a long time constant of 9 ± 3 ps. We speculate that the short time constant has the same origin as the fast component in the ordinary differential reflection. The long time constant reflects the relaxation of the valley and spin polarization. Hence, it is the valley and spin relaxation time. Similar results are obtained in several other fresh monolayer samples tested.

Next, we change the pump polarization to x. Since the linearly polarized light has two circular components of the same magnitude, it injects the same number of excitons to the two valleys, without a net valley or spin polarization. Consequently, no spin signal is observed, as confirmed in Fig. 3(d). Fig. 3(c) shows that the exciton recombination is not changed from Fig. 3(a). Hence, the exciton recombination rate is independent of the valley and spin polarization. Finally, we change the pump to σ^- to inject excitons with an opposite valley and spin polarization. As clearly shown in Fig. 3(f), the sign of the circular dichroism changes, while the dynamics remain the same. The differential reflection signal still remains unchanged, as shown in Fig. 3(e).

The valley-selective coupling illustrated in Fig. 1(d) holds only for monolayers. In bulk $MoSe_2$ with inversion symmetry, the valance bands are degenerate in both valleys, and hence the optical transitions become independent of valley. However, a circularly polarized pump still injects net spin polarization due to the spin-selection rules. Similarly, the circular dichroism of the probe still measures the spin polarization, but not the valley polarization. To study spin dynamics in bulk, we repeat the measurement summarized in Fig. 3 with a thick flake that is fabricated together with the monolayer flake and on the same substrate. The results are plotted in Fig. 4. No circular dichroism is detected, which suggests an ultrafast spin relaxation process in bulk. Without the spin–valley locking, spin relaxation can be induced by scattering events that do not involve intervalley transfer of excitons. Hence, a faster spin relaxation in bulk is expected. This further confirms that the spin–valley coupling in monolayer effectively increases the

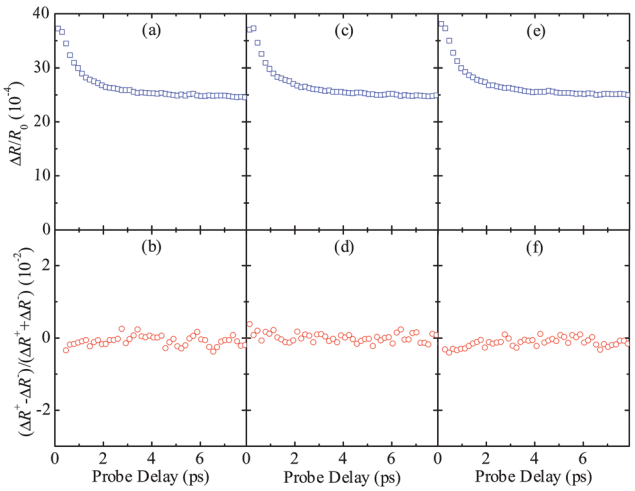

Fig. 4 Differential reflection (a, c, e) and the ratio between difference and sum of the two circular components (b, d, f) of bulk $MoSe_2$ measured with pump pulses of σ^+ (a, b), *x* (c, d), and σ^- (e, f) polarizations, respectively.

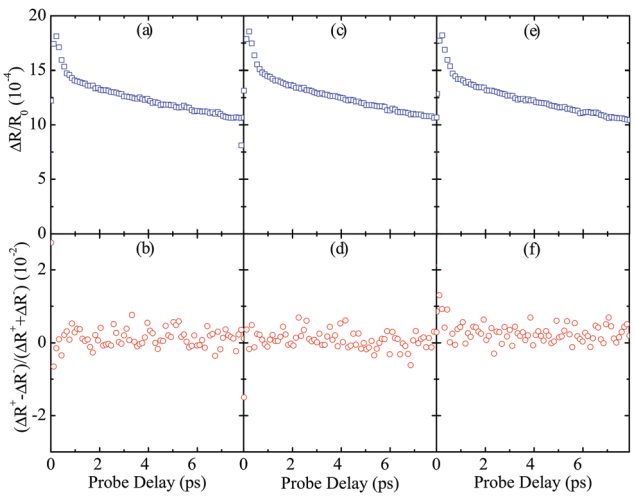

Fig. 5 Differential reflection (a, c, e) and the ratio between difference and sum of the two circular components (b, d, f) of a few-layer $MoSe_2$ flake with pump pulses of σ^+ (a, b), *x* (c, d), and σ^- (e, f) polarizations, respectively.

spin lifetime. In addition, the exciton lifetime is longer than monolayers, due to the indirect bandgap in bulk. We also study a few-layered flake as an intermediate case, which contains about 5–7 layers, estimated from its optical contrast. As shown in Fig. 5, no circular dichroism is detected, and the exciton lifetime is in between the values obtained from the bulk and monolayer samples.

Previously, the transient absorption technique had been used to study valley dynamics in MoS_2 monolayers at low temperatures.[38,39] Valley relaxation times of a few picoseconds and sub-picoseconds have been deduced from these measurements. Our study shows that a longer valley relaxation time can be achieved in $MoSe_2$ monolayers even at room temperature. Recently, several groups have observed circularly polarized photoluminescence in MoS_2 monolayers;[16,30–36,38,39] but there has been no report on such observations in $MoSe_2$. Based on our results, the exciton lifetime (130 ps) is much longer than the valley relaxation time (9 ps). Furthermore, since non-radiative recombination likely contributes to the lifetime too, the radiative recombination time can be expected to be even longer. Therefore, it is reasonable that time-integrated measurements cannot effectively detect circularly polarized photoluminescence.

We note that the detected peak signal of $(\Delta R^+ - \Delta R^-)/(\Delta R^+ + \Delta R^-)$ is only about 0.02. Although a circularly polarized pump is expected to inject 100% valley polarization, as dictated by the selection rules, such rules are relaxed when moving away from the K and K′ points (or the bottom of the bands), due to state mixing. In our measurements, the excitation access energy of the pump is about 120 meV. Hence, it is expected to inject excitons with a valley polarization lower than unity. Furthermore, according to eqn (5), the efficiency of using transient absorption to probe valley polarization is determined by the coefficients C_1 and C_2. In particular, if the mechanisms that cause transient absorption are dominated by valley- and spin-independent ones, such as screening effects, the values of C_1 and C_2 are expected to be close, resulting in low detection efficiency. Nevertheless, this does not change the result of the measurement of valley relaxation time.

4. Conclusions

We have performed the first experimental study on valley and spin dynamics in monolayer $MoSe_2$, an important member of the newly developed 2D crystals. We demonstrated optical injection of valley- and spin-polarized excitons in this material by a circularly polarized pulse, utilizing the unique optical selection rules of monolayer transition metal dichalcogenides. Evolution of the injected valley polarization is monitored by measuring dynamic circular dichroism of a probe pulse tuned to the exciton resonance. We obtained a valley relaxation time of 9 ± 3 ps at room temperature. Our study demonstrated a new 2D crystal for room temperature valleytronics and spintronics, and illustrated the prospects of using heterostructures formed by different 2D crystals for valleytronics and spintronics.

Acknowledgements

H. Z. acknowledges support from the US National Science Foundation (DMR-0954486, EPSCoR-1430493). D. H. and Y. W. acknowledge supports from the National Basic Research Program 973 of China (2011CB932700, 2011CB932703) and the Chinese Natural Science Foundation (61335006, 61378073).

References

1 Q. H. Wang, K. Kalantar-Zadeh, A. Kis, J. N. Coleman and M. S. Strano, *Nat. Nanotechnol.*, 2012, **7**, 699–712.
2 K. S. Novoselov, A. K. Geim, S. V. Morozov, D. Jiang, Y. Zhang, S. V. Dubonos, I. V. Grigorieva and A. A. Firsov, *Science*, 2004, **306**, 666–669.
3 K. S. Novoselov, D. Jiang, F. Schedin, T. J. Booth, V. V. Khotkevich, S. V. Morozov and A. K. Geim, *Proc. Natl. Acad. Sci. U. S. A.*, 2005, **102**, 10451–10453.
4 K. F. Mak, C. Lee, J. Hone, J. Shan and T. F. Heinz, *Phys. Rev. Lett.*, 2010, **105**, 136805.
5 A. Splendiani, L. Sun, Y. Zhang, T. Li, J. Kim, C. Y. Chim, G. Galli and F. Wang, *Nano Lett.*, 2010, **10**, 1271–1275.
6 K. F. Mak, K. He, C. Lee, G. H. Lee, J. Hone, T. F. Heinz and J. Shan, *Nat. Mater.*, 2013, **12**, 207–211.
7 B. Radisavljevic, A. Radenovic, J. Brivio, V. Giacometti and A. Kis, *Nat. Nanotechnol.*, 2011, **6**, 147–150.
8 B. Radisavljevic and A. Kis, *Nat. Mater.*, 2013, **12**, 815–820.
9 H. Qiu, T. Xu, Z. Wang, W. Ren, H. Nan, Z. Ni, Q. Chen, S. Yuan, F. Miao, F. Song, G. Long, Y. Shi, L. Sun, J. Wang and X. Wang, *Nat. Commun.*, 2013, **4**, 2642.
10 M. Shanmugam, T. Bansal, C. A. Durcan and B. Yu, *Appl. Phys. Lett.*, 2012, **100**, 153901.
11 H. S. Lee, S. W. Min, Y. G. Chang, M. K. Park, T. Nam, H. Kim, J. H. Kim, S. Ryu and S. Im, *Nano Lett.*, 2012, **12**, 3695–3700.
12 W. J. Zhang, J. K. Huang, C. H. Chen, Y. H. Chang, Y. J. Cheng and L. J. Li, *Adv. Mater.*, 2013, **25**, 3456–3461.
13 R. S. Sundaram, M. Engel, A. Lombardo, R. Krupke, A. C. Ferrari, P. Avouris and M. Steiner, *Nano Lett.*, 2013, **13**, 1416–1421.
14 S. Tongay, J. Zhou, C. Ataca, J. Liu, J. S. Kang, T. S. Matthews, L. You, J. B. Li, J. C. Grossman and J. Q. Wu, *Nano Lett.*, 2013, **13**, 2831–2836.
15 D. Xiao, G. B. Liu, W. Feng, X. Xu and W. Yao, *Phys. Rev. Lett.*, 2012, **108**, 196802.
16 T. Cao, G. Wang, W. P. Han, H. Q. Ye, C. R. Zhu, J. R. Shi, Q. Niu, P. H. Tan, E. Wang, B. L. Liu and J. Feng, *Nat. Commun.*, 2012, **3**, 887.
17 Z. Gong, G.-B. Liu, H. Yu, D. Xiao, X. Cui, X. Xu and W. Yao, *Nat. Commun.*, 2013, **4**, 2053.
18 S. A. Wolf, D. D. Awschalom, R. A. Buhrman, J. M. Daughton, S. von Molnar, M. L. Roukes, A. Y. Chtchelkanova and D. M. Treger, *Science*, 2001, **294**, 1488–1495.
19 I. Žutić, J. Fabian and S. Das Sarma, *Rev. Mod. Phys.*, 2004, **76**, 323.
20 S. Datta and B. Das, *Appl. Phys. Lett.*, 1990, **56**, 665.
21 J. Isberg, M. Gabrysch, J. Hammersberg, S. Majdi, K. K. Kovi and D. J. Twitchen, *Nat. Mater.*, 2013, **12**, 760–764.
22 Z. Y. Zhu, Y. C. Cheng and U. Schwingenschlogl, *Phys. Rev. B: Condens. Matter*, 2011, **84**, 153402.
23 A. Molina-Sanchez, D. Sangalli, K. Hummer, A. Marini and L. Wirtz, *Phys. Rev. B: Condens. Matter*, 2013, **88**, 045412.
24 L. F. Sun, J. X. Yan, D. Zhan, L. Liu, H. L. Hu, H. Li, B. K. Tay, J. L. Kuo, C. C. Huang, D. W. Hewak, P. S. Lee and Z. X. Shen, *Phys. Rev. Lett.*, 2013, **111**, 126801.
25 T. Cheiwchanchamnangij and W. Lambrecht, *Phys. Rev. B: Condens. Matter*, 2012, **85**, 205302.
26 W. X. Feng, Y. G. Yao, W. G. Zhu, J. J. Zhou, W. Yao and D. Xiao, *Phys. Rev. B: Condens. Matter*, 2012, **86**, 165108.
27 Z. Li and J. P. Carbotte, *Phys. Rev. B: Condens. Matter*, 2012, **86**, 205425.
28 X. Li, F. Zhang and Q. Niu, *Phys. Rev. Lett.*, 2013, **110**, 066803.
29 W. Y. Shan, H. Z. Lu and D. Xiao, *Phys. Rev. B: Condens. Matter*, 2013, **88**, 125301.
30 G. Kioseoglou, A. T. Hanbicki, M. Currie, A. L. Friedman, D. Gunlycke and B. T. Jonker, *Appl. Phys. Lett.*, 2012, **101**, 221907.
31 H. Zeng, J. Dai, W. Yao, D. Xiao and X. Cui, *Nat. Nanotechnol.*, 2012, **7**, 490–493.
32 K. F. Mak, K. He, J. Shan and T. F. Heinz, *Nat. Nanotechnol.*, 2012, **7**, 494–498.
33 G. Sallen, L. Bouet, X. Marie, G. Wang, C. R. Zhu, W. P. Han, Y. Lu, P. H. Tan, T. Amand, B. L. Liu and B. Urbaszek, *Phys. Rev. B: Condens. Matter*, 2012, **86**, 081301.
34 S. F. Wu, C. M. Huang, G. Aivazian, J. S. Ross, D. H. Cobden and X. D. Xu, *ACS Nano*, 2013, **7**, 2768–2772.
35 S. Wu, J. S. Ross, G.-B. Liu, G. Aivazian, A. Jones, Z. Fei, W. Zhu, D. Xiao, W. Yao, D. Cobden and X. Xu, *Nat. Phys.*, 2013, **9**, 149–153.
36 A. M. Jones, H. Y. Yu, N. J. Ghimire, S. F. Wu, G. Aivazian, J. S. Ross, B. Zhao, J. Q. Yan, D. G. Mandrus, D. Xiao, W. Yao and X. D. Xu, *Nat. Nanotechnol.*, 2013, **8**, 634–638.
37 D. Lagarde, L. Bouet, X. Marie, C. R. Zhu, B. L. Liu, T. Amand, P. H. Tan and B. Urbaszek, *Phys. Rev. Lett.*, 2014, **112**, 047401.
38 C. Mai, A. Barrette, Y. Yu, Y. G. Semenov, K. W. Kim, L. Cao and K. Gundogdu, *Nano Lett.*, 2013, **14**, 202–206.
39 Q. Wang, S. Ge, X. Li, J. Qiu, Y. Ji, J. Feng and D. Sun, *ACS Nano*, 2013, **7**, 11087–11093.
40 A. Castellanos-Gomez, N. Agraït and G. Rubio-Bollinger, *Appl. Phys. Lett.*, 2010, **96**, 213116.
41 M. M. Benameur, B. Radisavljevic, J. S. Héron, S. Sahoo, H. Berger and A. Kis, *Nanotechnology*, 2011, **22**, 125706.
42 P. Tonndorf, R. Schmidt, P. Bottger, X. Zhang, J. Borner, A. Liebig, M. Albrecht, C. Kloc, O. Gordan, D. R. T. Zahn, S. M. de Vasconcellos and R. Bratschitsch, *Opt. Express*, 2013, **21**, 4908–4916.
43 J. S. Ross, S. Wu, H. Yu, N. J. Ghimire, A. M. Jones, G. Aivazian, J. Yan, D. G. Mandrus, D. Xiao, W. Yao and X. Xu, *Nat. Commun.*, 2013, **4**, 1474.
44 S. Tongay, J. Zhou, C. Ataca, K. Lo, T. S. Matthews, J. B. Li, J. C. Grossman and J. Q. Wu, *Nano Lett.*, 2012, **12**, 5576–5580.

45 H. T. Wang, D. S. Kong, P. Johanes, J. J. Cha, G. Y. Zheng, K. Yan, N. A. Liu and Y. Cui, *Nano Lett.*, 2013, **13**, 3426–3433.
46 D. S. Kong, H. T. Wang, J. J. Cha, M. Pasta, K. J. Koski, J. Yao and Y. Cui, *Nano Lett.*, 2013, **13**, 1341–1347.
47 G. Cunningham, M. Lotya, C. S. Cucinotta, S. Sanvito, S. D. Bergin, R. Menzel, M. S. P. Shaffer and J. N. Coleman, *ACS Nano*, 2012, **6**, 3468–3480.
48 S. Schmitt-Rink, D. A. B. Miller and D. S. Chemla, *Phys. Rev. B: Condens. Matter*, 1987, **35**, 8113–8125.